
ELASTIC INTERACTION ENERGY-INFORMED REAL-TIME TRAFFIC SCENE PERCEPTION

Yaxin FENG¹, Yuan LAN¹, Luchan ZHANG^{2*}, Guoqing LIU^{3*} and Yang XIANG^{1,4*}

¹Department of Mathematics, Hong Kong University of Science and Technology,
Clear Water Bay, Hong Kong SAR, China

²College of Mathematics and Statistics, Shenzhen University, Shenzhen, China

³Shenzhen Youjia Innov Tech Co., Ltd., Shenzhen, China

⁴Algorithms of Machine Learning and Autonomous Driving Research Lab, HKUST Shenzhen-Hong Kong
Collaborative Innovation Research Institute, Futian, Shenzhen, China

{yfengba, ylanaa}@connect.ust.hk, zhanglc@szu.edu.cn, guoqing@minieye.cc, maxiang@ust.hk

ABSTRACT

Urban segmentation and lane detection are two important tasks for traffic scene perception. Accuracy and fast inference speed of visual perception are crucial for autonomous driving safety. Fine and complex geometric objects are the most challenging but important recognition targets in traffic scene, such as pedestrians, traffic signs and lanes. In this paper, a simple and efficient topology-aware energy loss function-based network training strategy named EIEGSeg is proposed. EIEGSeg is designed for multi-class segmentation on real-time traffic scene perception. To be specific, the convolutional neural network (CNN) extracts image features and produces multiple outputs, and the elastic interaction energy loss function (EIEL) drives the predictions moving toward the ground truth until they are completely overlapped. Our strategy performs well especially on fine-scale structure, *i.e.* small or irregularly shaped objects can be identified more accurately, and discontinuity issues on slender objects can be improved. We quantitatively and qualitatively analyze our method on three traffic datasets, including urban scene segmentation data Cityscapes and lane detection data TuSimple and CULane. Our results demonstrate that EIEGSeg consistently improves the performance, especially on real-time, lightweight networks that are better suited for autonomous driving.

1 INTRODUCTION

Semantic segmentation is a pixel-level classification of images, which is a dense perception task. Among them, the low-latency, high-efficiency segmentation model is widely used in the autonomous driving industry that requires real-time reasoning or limited computing resources, such as advanced driver assistance systems (ADAS) [1], drones [2], and mobile robots. In this work, we mainly focus on two traffic scene perception tasks for autonomous vehicles, *i.e.* urban scene segmentation and segmentation-based lane detection. In the urban scene, accurate multi-class semantic segmentation is required to distinguish the drivable areas (roads) from sidewalks, buildings, vehicles, pedestrians, traffic signs and so on [3, 4]. In the lane detection problem, the existence and location of different lane instances need to be inferred in real time, even when they are occluded by cars and crowd [1, 5].

At present, vast studies of visual perception focus on the improvement of neural network structure, such as deeper and denser networks [6, 7, 8] and attention-based methods such as vision-transformer [9, 10]. However, although complex network structures with huge number of parameters promise sophisticated performance, they will bring significant computational cost and have relatively slow inference speed. Thus these networks are not practical for many autonomous driving assistant systems that require real-time perception under limit computing resources [11]. Consequently, the study on real-time traffic scene perception on low compute devices are necessary.

*Corresponding author.

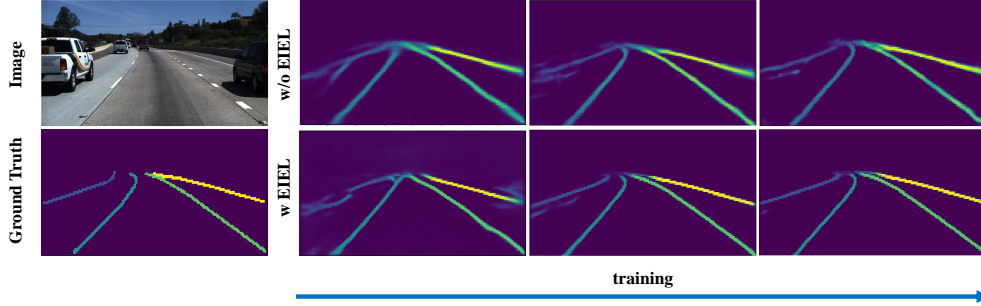


Figure 1: An example of training process. The pictures from left to right are the predictions of the models without/with EIEL during training. EIEL corrected the wrong classification pixels, and the end of the lane is clearer.

On the other hand, because the prediction errors often appear on geometry complex objects such as disconnected at/missing slender structures with only a few pixels inside, and blurry on boundaries of irregular shapes, another prevailing direction is to develop topology-aware approaches. The main branch of the boundary refinement methods is post processing [12, 13, 14], which will slow the inference speed. Another type of methods improve boundary segmentation during training, *e.g.* developing boundary-aware loss functions [15, 16, 17, 18, 19, 20, 21]. Our approach belongs to the second category, which utilizes a global topological-aware loss function to guide lightweight neural networks to extract more image features and global contextual information during the training phase, resulting in better performance compared to the baseline; see Fig. 1. We believe that our approach will also be effective in other visual perception tasks, and larger size models on other application such as high resolution image segmentation [22].

We propose a topology-aware loss-informed training strategy for multi-class semantic segmentation, named EIEGSeg (Elastic Interaction Energy Guided Segmentation). It is a plugged-in training strategy in the sense that our EIEL can be integrated in any network structures to improve the segmentation effect of complex geometries under class imbalance, without increasing computational complexity and inference time. Our loss function is inspired by the line defects of dislocation in crystals [23]. In image segmentation problems, this energy considers pixels of an object as a whole, rather than considering distance between pairwise pixels on the boundary, thus long-thin objects tend to be connected as the energy descends, and the edges of complex topological shapes are clearly outlined. Figure 2 shows some effective applications by adding EIEL on a baseline. Slender objects such as poles and occluded lane lines are better connected and identified, boundaries of small and irregular shape objects such as traffic sign, traffic light, pedestrians, riders, etc. can be clearer recognized. More details of the method will be provided in Sec. 3.2.

We evaluate our method on three popular autonomous driving scene benchmarks, *i.e.* one urban scene data Cityscapes [24] and two lane detection datasets Tusimple [25] and CULane [1]. We compare the performance based on a real-time network structure ERFNet [3], BiSeNetV1 [26] with or without EIEL function. A popular non-real time FCN semantic segmentation baseline HRNet-W48-OCR (OCR) [6] is also fine-tuned with EIEGSeg strategy. The experiment results show that training with EIEL can consistently improve the mIoU for segmentation, accuracy, F1-score for lane detection based on different network backbones.

The main contributions are as follow:

- We propose a simple and efficient topology-aware energy-based loss function EIEL for multi class segmentation. Small, slender and irregularly shaped objects can be identified more accurately, and discontinuity issues on slender objects can be significantly improved comparing with the baselines.
- The EIEGSeg training strategy is independent of network selection, and can be applied to any end-to-end network structure during training stage. Our approach works well on both lightweight and high-resolution networks, with prominent improvements in lightweight networks that are suitable for assisting autonomous vehicles in real-time inference.
- Three datasets are used to evaluate our method. In Cityscapes, the prediction accuracy on fine-scale structure objects boosts remarkably. In TuSimple and CULane, the lane segmentation is much clearer and the disconnection problem caused by occlusion is fixed.

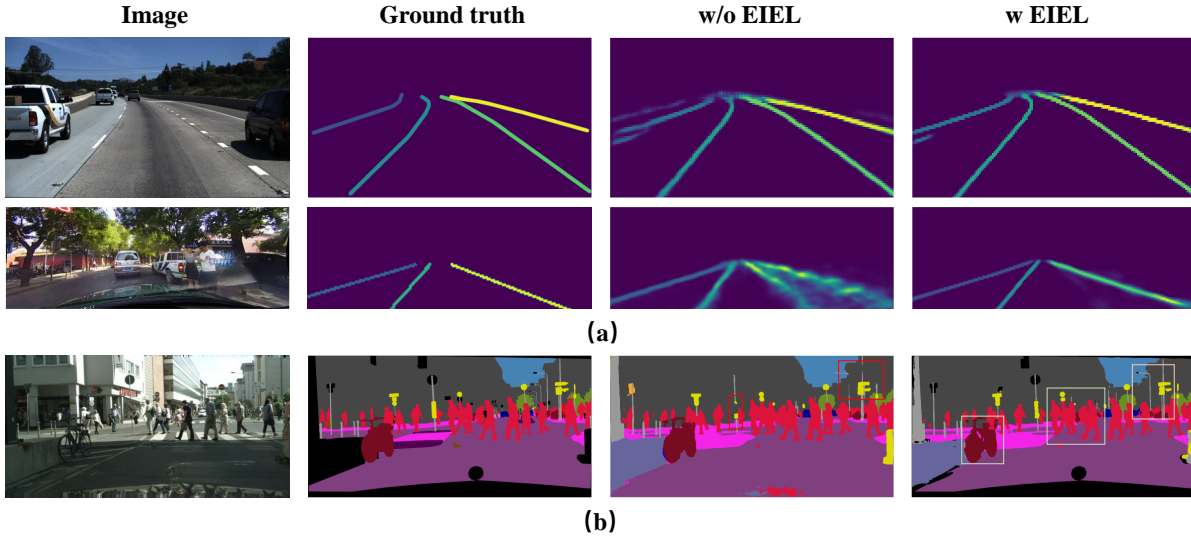


Figure 2: Comparison of the output maps between Baseline ERFNet [3] without (w/o) and with (w) EIEL in (a) lane detection and (b) segmentation. To be specific, the pictures from left to right are: raw image, ground truth, outputs w/o EIEL and outputs w EIEL.

2 RELATED WORK

2.1 Semantic Segmentation Network Structures

The fast development of end-to-end deep learning-based segmentation started from fully convolutional network (FCN) [27]. Many following works are based on this encoder-decoder network structure. In addition to those non-real time networks that have deeper and denser layers [28, 29, 7, 8] or transformer series attention-based network [10], more and more studies focus on design lightweight network delicately [3, 26, 4, 30, 31] and can achieve real-time performance that balances the effectiveness and the efficiency. In the lane segmentation problem, SCNN [1] proposes the spatial information passing network structure blocks, which can also be used in semantic segmentation.

2.2 Topology-aware segmentation

There are two branches of segmentation refinement, i.e., post-processing and applying topology-aware technique.

Post-refinement such as markov random fields (MRF) [12] and conditional random fields (CRFs) [13] refine the outputs of network. Clustering is utilized to distinguish the instances type in lane detection task after training [32]. Segfix [14] can transfer the interior pixels to be boundaries by training a separate network. However, the end-to-end network architecture without post-process performs better for real-time inference in most cases.

Some works on segmentation geometry refinement focus on object boundary. Pairwise pixel-level affinity fields have been used to classify different pixels, *e.g.* [15, 16, 19]. InverseForm [17] designs an inverse-transformation network to learn the boundaries distance. Loss functions in [20] are studied and proposed to refine the boundary details. Most of these training processes are combined with cross-entropy (CE) and fuse different layer features to improve the details. However, they are not examined on lightweight network architectures, thus remaining a question that whether they can significantly improve real-time networks. Also, most of these methods are not sensitive in long-thin or fine-scale objects.

Others methods focus on topology relation of pixels or refine the class imbalance problem. Intersection over union (IoU) is transformed into differentiable form loss function to guide the refinement of pixels prediction [33]. [21, 34] utilized elastic interaction energy loss function to achieve connection improvement on medical binary segmentation. [35] uses a topology-preserving loss function based on the thought of level set method and Betti number in conjunction with binary cross energy to improve the connectivity of slender objects, but it was only applied in binary problems, *e.g.* eye blood vessels, remote sensing data and road crack segmentation.

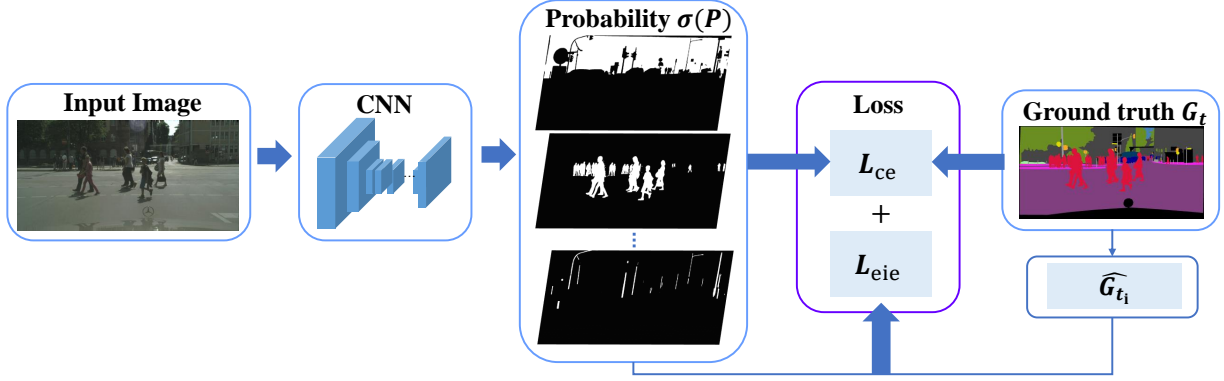


Figure 3: Network Structure of EIEGSeg, which jointly guided by EIEL and CE in the training process. Note that this is just a schematic illustration, and the predicted probability maps of some complicated cases in the figure do not exactly correspond to reality.

3 METHODOLOGY

3.1 Network Structure

The proposed strategy EIEGSeg is jointly trained by the guidance of EIEL and CE. The overall architecture of EIEGSeg is shown in figure 3. EIEL and CE are jointly applied in the training process, while the CE help classifying different categories of pixels and the EIEL refines the topology of each class. Since EIEGSeg is a multi-class segmentation based strategy, the network predicts N output maps for N -class objects and the ground truths are adjusted into the one-hot form when applying EIEL. The overall training strategies of our two visual perception tasks are similar, *i.e.* urban scene segmentation and lane detection, except that a post process is required in lane detection tasks, in which lane coordinates are collected from the predicted instance masks.

3.2 Elastic Interaction Energy

3.2.1 Preliminary

The elastic interaction energy functional defined in [23] is

$$E = \int_{\gamma} \int_{\gamma'} \frac{dl \cdot dl'}{r} \quad (1)$$

In the above functional, γ' is the curves with other parameter s' , vector dl represents line element on one set of curves γ with tangent direction τ , *i.e.* $dl = \tau dl$, and the r is Euclidean distance between (x,y) and (x',y') , *i.e.* $r = \sqrt{(x-x')^2 + (y-y')^2}$.

3.2.2 EIEL for Image Segmentation

In our tasks, we define the prediction γ_p and ground truth γ_{gt} between two sets of curves, and Eq. 1 becomes:

$$\begin{aligned} E &= E_s + E_i \\ &= \frac{1}{8\pi} \int_{\gamma_{gt} \cup \gamma_p} \int_{\gamma'_{gt} \cup \gamma'_p} \frac{dl \cdot dl'}{r} \\ &= \frac{1}{8\pi} \int_{\gamma_{gt}} \int_{\gamma'_{gt}} \frac{dl_{gt} \cdot dl'_{gt}}{r} + \frac{1}{8\pi} \int_{\gamma_p} \int_{\gamma'_p} \frac{dl_p \cdot dl'_p}{r} \\ &\quad + \frac{1}{4\pi} \int_{\gamma_{gt}} \int_{\gamma_p} \frac{dl_{gt} \cdot dl_p}{r}, \end{aligned} \quad (2)$$

where the vector dl is the sum of ground truth l_{gt} and the predicted l_p , and their directions are opposite, $dl = dl_{gt} + dl_p$.

In Eq. 2, the self-energy E_s consists of the first two terms for the self-energies of the prediction curve set γ_p and the ground truth curve set γ_{gt} , while the third term is the interaction energy E_i between the two sets of curves γ_p and γ_{gt} . Since the prediction curve γ_p and the ground truth curve γ_{gt} have opposite orientations, the elastic interaction between them is strongly attractive based on the third term in Eq. 2, and the prediction curve γ_p is attracted to the ground truth curve γ_{gt} to minimize the total energy in Eq. 2; see Fig.4 (a). When the two curves coincide, the energy minimum state is reached, and the ground truth is identified perfectly by the prediction. Under this elastic energy, the boundaries of the disconnected parts of the prediction are also attracted to each other for the same reason, and eventually combine; see Fig.4 (b). Besides, the self-energy of the prediction tends to make the prediction curves smoothing, because a longer curve has a larger self-energy. More mathematical properties of this elastic loss can be found in [21, 34].

In the image space, the boundary of ground truth G_t is expressed as $\nabla G_t = \nabla(G_t - 0.5) = -\delta(\gamma_{gt})\mathbf{n}_{gt}$. If the predicted probability of the moving predicted curves is p , the curves can be expressed implicitly by gradient of $\Phi_p = 0.5 - p$ ranging in $[-0.5, 0.5]$, i.e. $\nabla\Phi_p = -\delta(\gamma_p)\mathbf{n}_p$. Note that \mathbf{n}_{gt} and \mathbf{n}_p are unit normal vectors of curves (boundaries).

Thus, the elastic interaction energy functional as well as the EIE loss should be:

$$E(G_t, \Phi_p) = \frac{1}{8\pi} \int_{\mathbf{R}^2} dx dy \int_{\mathbf{R}^2} \frac{\nabla(G_t + \alpha\Phi_p)(x, y) \cdot \nabla(G_t + \alpha\Phi_p)(x', y')}{r} dx' dy' \quad (3)$$

In order to apply this loss function in neural network, the velocity field as well as the gradient descent direction is required in back propagation. After applying variation of the functional Eq. 3 about the prediction Φ_p , the velocity field of prediction obtained:

$$v(\Phi_p) = -\frac{\delta E}{\delta \Phi_p} = \frac{1}{4\pi} \int_{\Omega} \frac{\mathbf{r}}{r^3} \cdot \nabla(G_t + \alpha\Phi_p)(x', y') dx' dy' \quad (4)$$

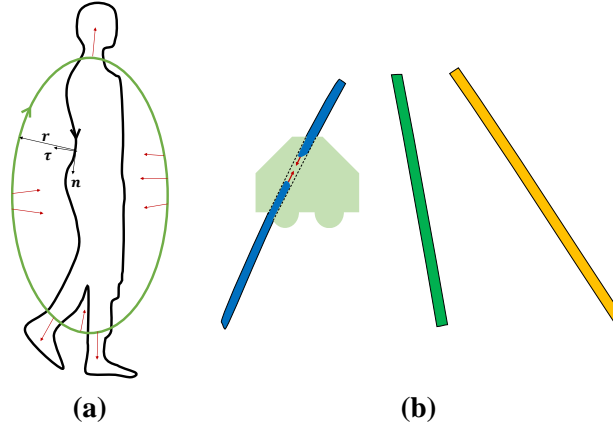


Figure 4: Description of how the EIEL works. (a) shows how the moving curve being attracted to the ground truth. (b) shows how the disconnected prediction of the left most lane is corrected by EIEL even it is occluded by a car.

3.2.3 EIEL-Guided Multi Class Segmentation

In multi class learning, N feature maps are output at the last layer of neural network. Each output map is represented by P_i and Softmax σ is applied to convert them into probability distribution of each pixel, i.e. $\sigma : P \rightarrow p \in [0, 1]^{N \times h \times w}$. Then the implicit function of predictions is $\Phi_i = 0.5 - \sigma(P)_i$, and the corresponding expression of ground truth with opposite orientation is $\hat{G}_{t_i} - 0.5$, where \hat{G}_{t_i} is the one-hot mode of the ground truth, $\hat{G}_{t_i} = \mathbf{1}_{G_{t_i}}$.

According to Eq. 3, the EIEL in multi-class segmentation is:

$$L_{eie} = \sum_i E(\sigma(P)_i, \hat{G}_{t_i}). \quad (5)$$

In N class semantic segmentation, each pixel on an image has a class label from 0 to $N - 1$, within which the background is class 0 (the background is classified as ignore-label 255 in segmentation task, thus some unpredicted

areas remain; see the last two columns in Fig 5). Therefore, the output layer has N feature prediction maps, i.e. the output size is $B * N * h * w$.

3.2.4 Efficient Calculation

As the energy function L_{eie} in Eq. 3 is an integral over the whole image domain, fast Fourier transform can make the computation more efficient, by which the computation cost is reduced from $O(N^2)$ to $O(N \log N)$. Assume the Fourier transform of $G_t + \alpha \Phi_p$ is d_{mn} , where m and n are frequencies in the Fourier space. The Fourier transform of $\frac{1}{R} = \frac{1}{\sqrt{x^2+y^2}}$ is $\hat{\frac{1}{R}} = \frac{1}{2\pi\sqrt{m^2+n^2}}$. Therefore, in the Fourier space, the EIEL can be transformed into the form as

$$L_{eie} = \sum_{m,n} \sqrt{m^2 + n^2} \cdot |d_{mn}|^2, \quad (6)$$

and the gradient of L_{eie} is the inverse Fourier transform, which is used in backward propagation

$$\frac{\delta L_{eie}}{\delta \Phi_p} = \mathcal{F}^{-1} \left(\frac{\sqrt{m^2 + n^2}}{2} d_{mn} \right). \quad (7)$$

3.2.5 Total loss function in EIEGSeg

The training loss L_t in EIEGSeg is

$$L_t = \lambda_1 L_{eie} + \lambda_2 L_{ce}(P, G_t). \quad (8)$$

where L_{eie} represents EIE loss and L_{ce} is the cross-entropy loss. $\lambda_i, i = 1, 2$ are parameters.

4 EXPERIMENTS

4.1 Implimentation Details

In semantic segmentation problem, we upsample the feature size and get end-to-end pixelwise prediction. The size of input images are H and W , and the output is with the size of $B * C * h * w$, where C is the number of output feature map, $h = H/s, w = W/s$.

In lane detection problems, we upsample the features into $1/4$ of the original size, i.e. $B * C * h * w$ where $s = 4$, because lanes are well structured, and do not need so many pixels to represent them. The ground truth is also down-scale to $1/4$ with linear interpolation. After segmentation, we chose the pixels in the center each row (sampling equidistant on the y -direction) of the lane line as their coordinates.

The experiments are implemented on a GPU RTX 4000 and RTX 3060.

4.2 Datasets and Evaluation Metrics

4.2.1 Cityscapes.

In Cityscapes [24], dense annotations with 19 object classes are provided. The training and validation data amount is 2975 and 500, and we use the validation data in testing. We apply the official metric mean Intesection-over-Union (mIoU) and the IoU of each class to measure the performance overall and in specific categories.

4.2.2 TuSimple.

Tusimple [25] has a maximum of five lane lines on highway and most of which are in daytime and clear weather, which includes 3626 training data and 2782 testing data. The official metric of the TuSimple dataset is accuracy (Acc), the false positive (FP) and the false negative (FN) are evaluated. In addition, we also compute the F1 score, and the average pixel-wise F1 score (Pix. F1) of the predictions. The Acc defined in TuSimple benchmark is: $Acc = \frac{N_{pred}}{N_{gt}}$, where N_{pred} is the number of correct predicted lane points and N_{gt} is the amount of ground-truth lane points.

4.2.3 CULane.

CULane [1] includes eight difficult-to-detect urban environments such as crowded, darkness, no-line, and shadows, and marks up to four lane lines. Data volume is 88880/9675/34680 as train/val/test. The official metric for CULane is F1 score based on IoU: $F1 = 2 \cdot \left(\frac{P \cdot R}{P + R} \right)$, where P defined as $\frac{TP}{TP + FP}$, R defined as $\frac{TP}{TP + FN}$. TP is the correctly predicted lane points, FP is the false positives number, and FN is false negatives ones.

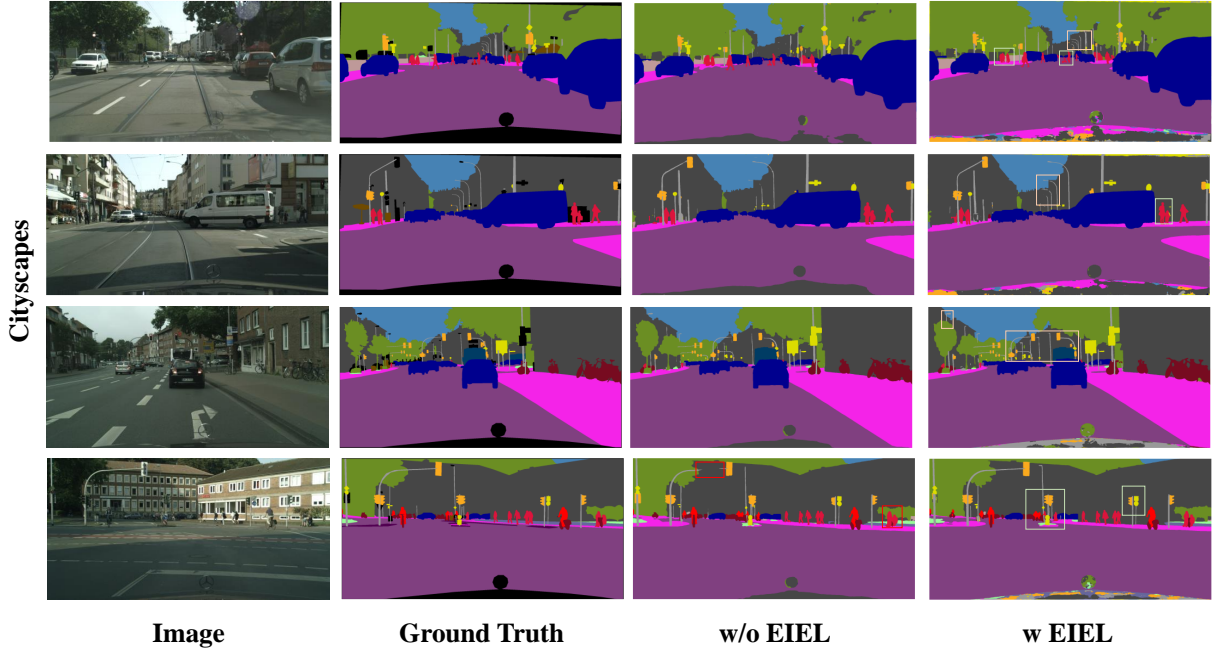


Figure 5: Comparison of the performance on Semantic Segmentation task. The pictures above from left to right are ground truth, label, baseline OCR without (w/o) and with (w) EIEL. Orange boxes indicate the better performance on pole, traffic sign and light, and the green ones are those with clearer pedestrians segmentation. Some obvious incorrect segmentation positions (w/o EIEL) in the third column are highlighted in red boxes.

4.3 Results

4.3.1 Semantic segmentation.

Table 1 shows performance on Cityscapes validation dataset. As shown in Tab.1, the predictions of wall, pole, traffic light, traffic sign, pedestrian, rider, bicycle are improved consistently when using different backbones with EIEL.

Table 1: Class-wise mIoU results on Cityscapes validation set. First seven rows are real-time approaches, and the last seven rows are non real-time ones. \dagger are our implementation. * means the results of multi-scale inference.

Method	road	side-walk	bldg.	wall	fence	pole	traffic light	traffic sign	veg.	terrian	sky	person	rider	car	truck	bus	train	motor	bicycle	mIoU
ENet [36]	96.3	74.2	85.0	32.2	33.2	43.5	34.1	44.0	88.6	61.4	90.5	65.5	38.4	90.6	36.9	50.5	48.1	38.8	55.4	58.3
LED [30]	98.1	79.5	91.6	47.7	49.9	62.8	61.3	72.8	92.6	61.2	94.9	76.2	53.7	90.9	64.4	64.0	52.7	44.4	71.6	70.6
LBNAE [31]	98.2	84.0	91.6	50.7	49.5	60.9	69.0	73.6	92.6	70.3	94.4	83.0	65.7	94.9	62.0	70.9	53.3	62.5	71.8	70.65
ERF \dagger [3]	97.46	80.79	90.28	49.5	55.6	60.46	61.48	70.33	91.07	61.65	93.3	74.12	54.5	92.14	62.24	73.55	60.34	45.18	68.44	70.65
EIEGSeg(ERF) \dagger	97.69	80.46	91.57	58.48	53.19	65.36	66.86	74.69	92.21	63.86	94.06	78.72	59.76	93.66	71.08	77.68	64.93	46.55	72.1	73.84
BSV1 \dagger [26]	97.93	83.42	91.70	47.21	52.44	63.13	70.41	77.76	91.99	61.64	94.73	80.64	59.60	94.50	73.23	83.25	74.07	58.34	75.96	75.37
EIEGSeg(BSV1) \dagger	98.05	84.45	92.42	55.27	59.05	65.52	70.97	78.84	92.38	63.48	94.92	81.40	61.80	94.52	66.47	79.43	72.82	52.53	76.43	75.83
LargeFOV [37]	98.3	78.8	89.9	42.2	52.2	52.9	62.3	71.1	91.0	59.2	92.2	75.9	52.1	92.3	48.8	70.2	37.6	54.6	72.3	68.0
SCNN(R101) [11]	98.3	86.1	92.6	46.7	61.2	66.1	74.3	81.5	92.7	65.4	94.7	84.0	65.5	94.8	57.7	82.0	59.9	67.0	80.1	76.4
DeepLabV3 [38]	98.4	86.5	93.1	63.9	62.6	66.1	72.2	80.0	92.8	66.3	95.0	83.3	65.5	95.3	74.5	89.0	80.0	67.4	78.4	79.5
OCR [6]	98.52	87.5	93.67	62.15	66.47	71.6	75.48	82.62	93.32	66.31	95.04	84.69	66.76	95.90	86.58	91.59	86.58	69.39	79.70	81.60
EIEGSeg(OCR) \dagger	98.44	87.3	93.54	63.27	65.81	72.3	75.71	83.71	93.08	65.51	94.78	85.19	69.33	95.91	85.15	88.87	84.49	69.80	80.12	81.70
OCR*	98.61	88.11	93.94	65.67	67.51	72.67	77.00	84.05	93.58	67.75	95.11	85.66	68.44	96.24	88.05	92.73	86.13	71.16	80.91	82.80
EIEGSeg(OCR)* \dagger	98.61	88.39	93.94	66.71	68.37	73.95	77.67	85.06	93.45	69.26	95.00	86.38	71.12	96.20	81.36	91.61	84.99	71.53	81.39	82.90

As most of the autonomous driving scenarios require real-time performance, we firstly chose two popular lightweight CNN architectures ERFNet and BiSeNetV1-R18 (R18 is ResNet18) as backbones, whose inference speed is 83 and

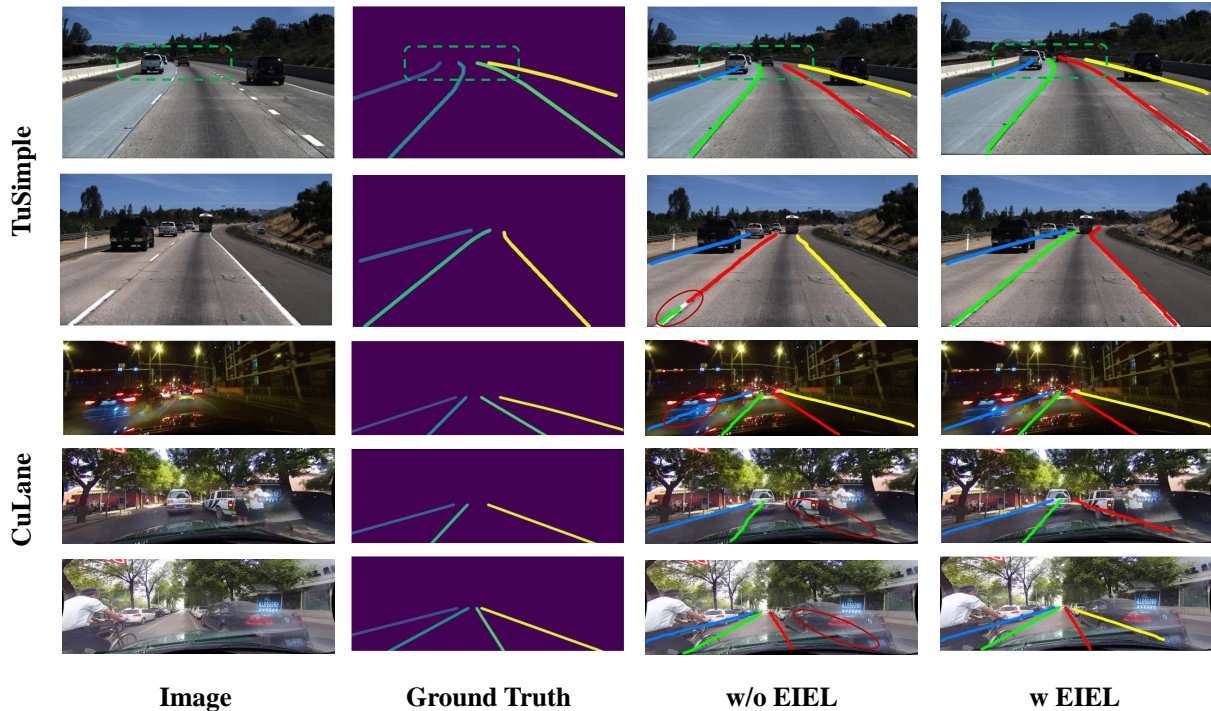


Figure 6: Performance on Lane Detection task with backbone ERFNet. From top to bottom, the baseline without EIEL are not curvy enough, line disconnected caused by wrong classify, bend as feature map blurry, lane missing caused by occlusion.

65.5 frames per second (FPS) on GPU, respectively [3, 26], see Tab. 1. It is noticed that our loss achieves a significant improvement of mIoU on baseline ERFNet (after 150 epoch of training until convergence), up to 3.19%. BiSeNetV2 [4] is an improved version of BiSeNetV1 with some auxiliary heads on training stage to gain better feature representation ability. Its large version, BiSeNetV2-L has a slower inference speed of FPS 47.3 but lower mIoU of 75.80 compared to EIEGSeg(BSV1) (75.82). This shows that our loss function can guide lightweight networks to better extract detailed features and thus get finer results on exquisite-structures. When using multi-scale inference (random scale on $\{0.25, 0.5, 0.75, 1.0, 1.25, 1.5, 1.75, 2.0\}$), EIEGSeg achieves 79.0 on backbone BiSeNetV1 (78.86 originally), which outperforms many other models.

In addition, our methods works well on larger size model, such as OCR, a high-resolution non real-time network structure with dense connections and of 0.15 FPS [39]. We use the pre-trained model provided by the author and add EIEL to continue the training. In our implementation, our method outperforms the pre-trained model, especially on fine-scale structures. Some other non real-time approaches are compared in the last six rows, while the single-scale and multi-scale test results are displayed in last for rows of 1.

Figure 5 shows semantic segmentation performance on cityscapes. The improved areas trained with EIEL are framed in different colors (the forth column). In the row 2 of right most column, the segmentation of the pedestrian legs is even better than what was provided in ground truth, because EIEGSeg correctly predicts the man in the picture wearing shorts with a gap between his legs.

4.3.2 Segmentation-based lane detection.

Figure 1 shows the training process with/without EIEL. The image and down-scaled ground truth are shown in Fig. 3. As our size of ground truth is $88 * 160$, the prediction boundaries are also grid-like. The first column is the model outputs after 1st epoch, which are both disconnected on the left most lane and blurry on the right most lane, because they are occluded by cars. Adding EIEL fixes the wrong prediction and finally the lanes are all continuous after convergence. In addition, EIEL makes the prediction much straighter, sharper and precise on details than those without EIEL.

Table 2: Comparison of class IoU and total IoU (threshold = 0.5) on baseline ERFNet with / without EIEL on CULane.

Method	Normal	Crowded	Dazzle	Shadow	No line	Arrow	Curve	Cross	Night	Total
ERF [3]	85.60	67.14	59.40	60.72	44.07	78.99	60.79	1861	61.61	68.82
EIEGSeg(ERF)	88.96	71.29	62.66	72.69	47.26	84.14	60.55	2795	66.41	72.19
EIEGSeg(ERF)+IoU+LE	90.08	72.21	63.58	72.96	48.95	85.58	62.46	2201	68.50	73.76

Table 3: Comparison of two baseline with / without EIEL on TuSimple. The batch size is set to be 8 and the training epoch is set 20.

Model	Acc (%)	FP	FN	F1	Pix.F1
ERFNet [3]	94.91	0.061	0.069	93.52	98.04
EIEGSeg(ERFNet)	95.16	0.061	0.062	93.81	98.30

It is noticed that in Fig. 6, our approach can make the shape at the end of the driveway clearer, and improve the mis-classification problem and lane blurry/missing situation. As marked in the pictures in the images, the far lane shape in the first row of images is curved, and the blocked lane line in the third row of image is straight, and our inference accuracy is higher. The disconnection due to incorrect classification in the second row, and the missing lane lines due to occlusion in the fourth and fifth rows are also fixed. The experiments shows that EIEL can indeed improve the details segmentation, and have better inference ability in poor visual conditions.

Table 2 and 3 shows the results on lane predictions of CULane and Tusimple, respectively. In CULane results, most of the category IoU increase with the assistance of EIEL as displayed in first two rows of Tab. 2. Last row in Tab.2 is the results when adding two auxiliary loss functions L_{IoU} and L_{exist} , where the former one guides the network to increase the pixel interaction of union, and the latter one is achieved by add an auxiliary branch of lane existence (LE), and calculated by binary cross entropy [1]. In experiment results of Tusimple, EIEL makes consistently improvement on every metrics shown in Tab. 3. These results show that the use of EIEL can significantly improve lane segmentation results and is suitable for any task that requires to obtain lane heat maps/probability maps. There are many other ways to tune the parameters, including setting the tusimple labels (5 lanes from left to fight, or 4 / 6 lanes on two sides of ego lane), batch size, learning rates, adding various auxiliary branches, etc. We do not focus too much on these improvement measures, but just make comparison on segmentation quality via experiments on the same code and machine until convergence.

Figure 7 shows some curves of the training process. The left column are validation losses, and the right column are average pixel accuracy and F1 measure. (a) and (b) are the experimental diagrams without EIEL, and (c) and (d) are the experimental diagrams with EIEL. Our EIEGSeg achieves early convergence (from about epoch 10), while the baseline curve oscillations do not flatten out until epoch 20. Due to the long-range nature of our loss, the model EIEGSeg, is insensitive to the initial distribution and has the properties of training stability and rapid convergence.

5 CONCLUSION

We proposed an EIEGSeg training strategy for multi class segmentation task in autonomous driving. It is proved to be robust on segmentation of geometry complex objects such as long-thin, small or irregular shaped objects. It can also be easily combined into different network architectures, especially the light-wight backbones, which can help achieve real-time inference in autonomous driving.

Acknowledgement

This work is supported by the Project of Hetao Shenzhen-HKUST Innovation Cooperation Zone HZQBKCZYB-2020083, the project Study on Algorithms for Traffic Target Recognition in Autonomous Driving at HKUST Shenzhen Research Institute and Shenzhen Science and Technology Program (No. KQTD20180411143338837).

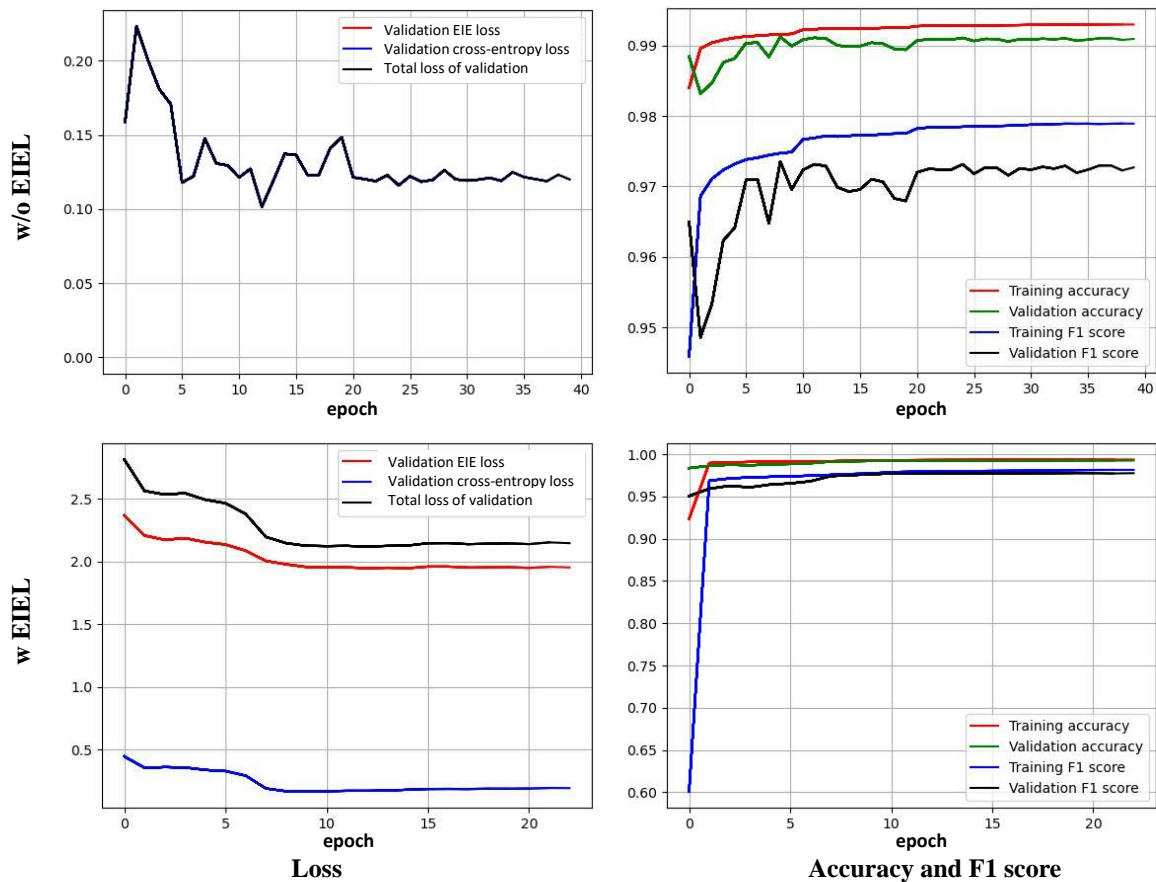


Figure 7: Illustration on how EIEL jointly trained with CE influences the loss value and pixel accuracy. EIEGSeg training strategy converges faster.

References

- [1] Xingang Pan, Jianping Shi, Ping Luo, Xiaogang Wang, and Xiaoou Tang. Spatial as deep: Spatial cnn for traffic scene understanding. In *Proceedings of the AAAI Conference on Artificial Intelligence*, volume 32, 2018.
- [2] Haobin Tan, Chang Chen, Xinyu Luo, Jiaming Zhang, Constantin Seibold, Kailun Yang, and Rainer Stiefelhagen. Flying guide dog: Walkable path discovery for the visually impaired utilizing drones and transformer-based semantic segmentation. In *2021 IEEE International Conference on Robotics and Biomimetics (ROBIO)*, pages 1123–1128. IEEE, 2021.
- [3] Eduardo Romera, José M Alvarez, Luis M Bergasa, and Roberto Arroyo. Erfnet: Efficient residual factorized convnet for real-time semantic segmentation. *IEEE Transactions on Intelligent Transportation Systems*, 19(1):263–272, 2017.
- [4] Changqian Yu, Changxin Gao, Jingbo Wang, Gang Yu, Chunhua Shen, and Nong Sang. Bisenet v2: Bilateral network with guided aggregation for real-time semantic segmentation. *International Journal of Computer Vision*, 129:3051–3068, 2021.
- [5] Yuenan Hou, Zheng Ma, Chunxiao Liu, and Chen Change Loy. Learning lightweight lane detection cnns by self attention distillation. In *Proceedings of the IEEE/CVF international conference on computer vision*, pages 1013–1021, 2019.
- [6] Yuhui Yuan, Xilin Chen, and Jingdong Wang. Object-contextual representations for semantic segmentation. In *Computer Vision—ECCV 2020: 16th European Conference, Glasgow, UK, August 23–28, 2020, Proceedings, Part VI 16*, pages 173–190. Springer, 2020.

- [7] Jingdong Wang, Ke Sun, Tianheng Cheng, Borui Jiang, Chaorui Deng, Yang Zhao, Dong Liu, Yadong Mu, Mingkui Tan, Xinggang Wang, et al. Deep high-resolution representation learning for visual recognition. *IEEE transactions on pattern analysis and machine intelligence*, 43(10):3349–3364, 2020.
- [8] Alexander Kirillov, Eric Mintun, Nikhila Ravi, Hanzi Mao, Chloe Rolland, Laura Gustafson, Tete Xiao, Spencer Whitehead, Alexander C Berg, Wan-Yen Lo, et al. Segment anything. In *Proceedings of the IEEE/CVF International Conference on Computer Vision*, pages 4015–4026, 2023.
- [9] Kai Han, Yunhe Wang, Hanting Chen, Xinghao Chen, Jianyuan Guo, Zhenhua Liu, Yehui Tang, An Xiao, Chunjing Xu, Yixing Xu, et al. A survey on vision transformer. *IEEE transactions on pattern analysis and machine intelligence*, 45(1):87–110, 2022.
- [10] Alexey Dosovitskiy, Lucas Beyer, Alexander Kolesnikov, Dirk Weissenborn, Xiaohua Zhai, Thomas Unterthiner, Mostafa Dehghani, Matthias Minderer, Georg Heigold, Sylvain Gelly, et al. An image is worth 16x16 words: Transformers for image recognition at scale. *arXiv preprint arXiv:2010.11929*, 2020.
- [11] Hojun Son and James Weiland. Lightweight semantic segmentation network for semantic scene understanding on low-compute devices. In *2023 IEEE/RSJ International Conference on Intelligent Robots and Systems (IROS)*, pages 62–69. IEEE, 2023.
- [12] Andrew Blake, Pushmeet Kohli, and Carsten Rother. *Markov random fields for vision and image processing*. MIT press, 2011.
- [13] John Lafferty, Andrew McCallum, Fernando Pereira, et al. Conditional random fields: Probabilistic models for segmenting and labeling sequence data. In *Icml*, volume 1, page 3. Williamstown, MA, 2001.
- [14] Yuhui Yuan, Jingyi Xie, Xilin Chen, and Jingdong Wang. Segfix: Model-agnostic boundary refinement for segmentation. In *Computer Vision—ECCV 2020: 16th European Conference, Glasgow, UK, August 23–28, 2020, Proceedings, Part XII 16*, pages 489–506. Springer, 2020.
- [15] Tsung-Wei Ke, Jyh-Jing Hwang, Ziwei Liu, and Stella X Yu. Adaptive affinity fields for semantic segmentation. In *Proceedings of the European conference on computer vision (ECCV)*, pages 587–602, 2018.
- [16] Henghui Ding, Xudong Jiang, Ai Qun Liu, Nadia Magnenat Thalmann, and Gang Wang. Boundary-aware feature propagation for scene segmentation. In *Proceedings of the IEEE/CVF International Conference on Computer Vision*, pages 6819–6829, 2019.
- [17] Shubhankar Borse, Ying Wang, Yizhe Zhang, and Fatih Porikli. Inverseform: A loss function for structured boundary-aware segmentation. In *Proceedings of the IEEE/CVF conference on computer vision and pattern recognition*, pages 5901–5911, 2021.
- [18] Chi Wang, Yunke Zhang, Miaomiao Cui, Peiran Ren, Yin Yang, Xuansong Xie, Xian-Sheng Hua, Hujun Bao, and Weiwei Xu. Active boundary loss for semantic segmentation. In *Proceedings of the AAAI Conference on Artificial Intelligence*, volume 36, pages 2397–2405, 2022.
- [19] Hoel Kervadec, Jihene Bouchtiba, Christian Desrosiers, Eric Granger, Jose Dolz, and Ismail Ben Ayed. Boundary loss for highly unbalanced segmentation. In *International conference on medical imaging with deep learning*, pages 285–296. PMLR, 2019.
- [20] Towaki Takikawa, David Acuna, Varun Jampani, and Sanja Fidler. Gated-scnn: Gated shape cnns for semantic segmentation. In *Proceedings of the IEEE/CVF international conference on computer vision*, pages 5229–5238, 2019.
- [21] Yuan Lan, Yang Xiang, and Luchan Zhang. An elastic interaction-based loss function for medical image segmentation. In *Medical Image Computing and Computer Assisted Intervention—MICCAI 2020: 23rd International Conference, Lima, Peru, October 4–8, 2020, Proceedings, Part V 23*, pages 755–764. Springer, 2020.
- [22] Tiancheng Shen, Yuechen Zhang, Lu Qi, Jason Kuen, Xingyu Xie, Jianlong Wu, Zhe Lin, and Jiaya Jia. High quality segmentation for ultra high-resolution images. In *Proceedings of the IEEE/CVF conference on computer vision and pattern recognition*, pages 1310–1319, 2022.
- [23] John Price Hirth, Jens Lothe, and Toshio Mura. Theory of dislocations. *Journal of Applied Mechanics*, 50(2):476–477, 1983.
- [24] Marius Cordts, Mohamed Omran, Sebastian Ramos, Timo Rehfeld, Markus Enzweiler, Rodrigo Benenson, Uwe Franke, Stefan Roth, and Bernt Schiele. The cityscapes dataset for semantic urban scene understanding. In *Proceedings of the IEEE conference on computer vision and pattern recognition*, pages 3213–3223, 2016.
- [25] TuSimple. Tusimple benchmark. <https://github.com/TuSimple/tusimple-benchmark>, 2017.

- [26] Changqian Yu, Jingbo Wang, Chao Peng, Changxin Gao, Gang Yu, and Nong Sang. Bisenet: Bilateral segmentation network for real-time semantic segmentation. In *Proceedings of the European conference on computer vision (ECCV)*, pages 325–341, 2018.
- [27] Jonathan Long, Evan Shelhamer, and Trevor Darrell. Fully convolutional networks for semantic segmentation. In *Proceedings of the IEEE conference on computer vision and pattern recognition*, pages 3431–3440, 2015.
- [28] Salih Can Yurtkulu, Yusuf Hüseyin Şahin, and Gozde Unal. Semantic segmentation with extended deeplabv3 architecture. In *2019 27th Signal Processing and Communications Applications Conference (SIU)*, pages 1–4. IEEE, 2019.
- [29] Zongwei Zhou, Md Mahfuzur Rahman Siddiquee, Nima Tajbakhsh, and Jianming Liang. Unet++: Redesigning skip connections to exploit multiscale features in image segmentation. *IEEE transactions on medical imaging*, 39(6):1856–1867, 2019.
- [30] Yu Wang, Quan Zhou, Jia Liu, Jian Xiong, Guangwei Gao, Xiaofu Wu, and Longin Jan Latecki. Lednet: A lightweight encoder-decoder network for real-time semantic segmentation. In *2019 IEEE international conference on image processing (ICIP)*, pages 1860–1864. IEEE, 2019.
- [31] Genshun Dong, Yan Yan, Chunhua Shen, and Hanzi Wang. Real-time high-performance semantic image segmentation of urban street scenes. *IEEE Transactions on Intelligent Transportation Systems*, 22(6):3258–3274, 2020.
- [32] Hala Abualsaud, Sean Liu, David B Lu, Kenny Situ, Akshay Rangesh, and Mohan M Trivedi. Laneaf: Robust multi-lane detection with affinity fields. *IEEE Robotics and Automation Letters*, 6(4):7477–7484, 2021.
- [33] Maxim Berman, Amal Rannen Triki, and Matthew B Blaschko. The lovász-softmax loss: A tractable surrogate for the optimization of the intersection-over-union measure in neural networks. In *Proceedings of the IEEE conference on computer vision and pattern recognition*, pages 4413–4421, 2018.
- [34] Yang Xiang, Albert CS Chung, and Jian Ye. An active contour model for image segmentation based on elastic interaction. *Journal of computational physics*, 219(1):455–476, 2006.
- [35] Xiaoling Hu, Fuxin Li, Dimitris Samaras, and Chao Chen. Topology-preserving deep image segmentation. *Advances in neural information processing systems*, 32, 2019.
- [36] Adam Paszke, Abhishek Chaurasia, Sangpil Kim, and Eugenio Culurciello. Enet: A deep neural network architecture for real-time semantic segmentation. *arXiv preprint arXiv:1606.02147*, 2016.
- [37] Liang-Chieh Chen, George Papandreou, Iasonas Kokkinos, Kevin Murphy, and Alan L Yuille. Deeplab: Semantic image segmentation with deep convolutional nets, atrous convolution, and fully connected crfs. *IEEE transactions on pattern analysis and machine intelligence*, 40(4):834–848, 2017.
- [38] Liang-Chieh Chen, George Papandreou, Florian Schroff, and Hartwig Adam. Rethinking atrous convolution for semantic image segmentation. *arXiv preprint arXiv:1706.05587*, 2017.
- [39] Seonkyeong Seong and Jaewan Choi. Semantic segmentation of urban buildings using a high-resolution network (hrnet) with channel and spatial attention gates. *Remote Sensing*, 13(16):3087, 2021.